UNIVERSITY OF MISKOLC

FACULTY OF MECHANICAL ENGINEERING AND INFORMATICS

ANALYSIS AND EVALUATION OF COATING CHARACTERISTICS

Booklet of PhD Theses

PREPARED BY:

OKHUNJON SAYFIDINOV

ISTVÁN SÁLYI DOCTORAL SCHOOL

TOPIC FIELD OF ENGINEERING MATERIAL SCIENCE, PRODUCTION SYSTEMS AND PROCESSES

TOPIC GROUP OF MATERIALS ENGINEERING AND MECHANICAL TECHNOLOGY

HEAD OF DOCTORAL SCHOOL

DR. GABRIELLA BOGNÁR

HEAD OF TOPIC GROUP

DR. GABRIELLA BOGNÁR

SCIENTIFIC SUPERVISOR

Dr. Gabriella Bognár

Miskolc

2023

1. INTRODUCTION

One of the successful equations for describing a class of dynamic nonlinear phenomena is the Kardar–Parisi–Zhang (KPZ) equation [1]. The application of this equation varies widely in topics such as vapour deposition, directed polymers, bacterial colony growth and superconductors [2], [3]. There are a number of computational studies related to discrete model simulations such as the Eden model, ballistic deposition models [4-9] and directed polymer model. All of these provide important features in the physical processes through simulation efficiency. The introduction of direct numerical integration is also an important point that requires more intensive computations. The first large scale numerical integration of the KPZ equation was performed by Amar and Family and the discrete Gaussian model was verified in [10]. Later, Moser improved his accuracy with further works [11-12]. However, the KPZ equation is not just a nonlinear equation that is applied by a similar method. To verify the theoretical predictions, numerical and analytical investigations are performed for the KPZ equation with correlated noise [13] and with quenched noise in anisotropic media [14], or in reaction–diffusion systems with multiplicative noise [15], for the Kuramato–Shivashisky equation (KS) of flame front propagation [16-17] and for the epitaxial growth equation [18].

In general, the direct approach to studying the growth equation is numerical integration and it can be seen as the ideal form of the equation that allows us to fully control the investigation. Unfortunately, Newman and Bray [19] reported some disadvantageous properties of the conventional numerical integration scheme, such as instability and an unphysical fixed point. Later works [20-21] reported that during numerical simulation instability can occur even in the case of small time steps. Lam and Shin [22] found that direct numerical integration by conventional finite difference schemes actually do not approximate the continuum KPZ equation. Previously, Amar and Family [23] integrated a similar equation using a generalized nonlinear term. The scaling behaviour of the KPZ equation was in most cases found to be different from the continuum equation. They even explained the results of their studies on KPZ nonlinear terms combining the effects of noise and nonlinearity.

In the last 30 years, different kinds of numerical methods have been proposed for the KPZ equation. These were implemented with various discretizing formulas of the nonlinear term. However, the diffusion term was mostly handled by the most standard Forward Time Centred Space (FTCS), where the time discretisation is based on the explicit Euler method.

The application of the discrete variational formulation to the KPZ equation has been discussed. An alternative approach to other well-known techniques, the variational analytical solutions of KPZ were introduced by Wio et al. in [24-26] and non-equilibrium potential has been obtained to

understand radial growth on a growing domain. In [24], a relation between the real-space discretisation schemes was examined. The authors provided discrete schemes of the KPZ equation, and they discussed the role of the Galilean invariance for discrete representations. In [26], the properties of a functional related to the KPZ equation are investigated. The main result is a path integral scheme; and, the authors defined expressions for the probability of entropy production along a trajectory and they obtained integral fluctuation theorems.

The thermodynamic uncertainty relation for the (1 + 1) dimensional Kardar–Parisi–Zhang equation on a finite spatial interval was considered by Niggeman and Seifert [27]. Numerical simulations compared with theoretical predictions showed convincing agreement.

Cartes et al. [28] studied the analytical laws of the scale-dependent correlation time to follow the expected crossover from the short-distance Edwards–Wilkinson scaling to the universal long-distance Kardar–Parisi–Zhang scaling.

The mathematical model derived from this equation can serve as a starting point for exploring ultra-thin film coatings with complex properties arising from the film growth process, such as porosity and pinholes. [29]. In terms of medical surface coating applications, such as stent coatings [29], this equation can simulate the process and has potential value in advancing our understanding and improvement of such surface growth. However, since the equation only has exact exponents for one-dimensional cases, additional numerical analysis and simulations are necessary to accurately characterize these processes..

The critical importance of controlling the surface during film deposition is demonstrated by adjusting parameters such as roughness, porosity, and thickness of the films. The use of computer simulations is becoming increasingly useful for precision control, therefore requiring further research to improve thin film deposition techniques and procedures.

2. IMPACT OF THE INITIAL SURFACE MORPHOLOGY

2.1. Results without noise term

Simulations have been carried out by MATLAB R2019a. Numerical solution for height profiles are calculated with the following data: $x \in [-200, 200]$, $t \in [0, 10000], N = 100, \Delta t = 1/100$, where N denotes the number of division points on the x-axis and Δt is the time step.

In the resulted figures below the complete solutions of the KPZ Eq. (2.1)

$$\frac{\partial h}{\partial t}(x,t) = \nu \nabla^2 h(x,t) + \frac{\lambda}{2}(\nabla h)^2 + \eta(x,t), \tag{2.1}$$

that have been presented for different initial condition and various amplitudes. However, for simplicity, the parameters are chosen as $\nu = \lambda = 0.1$ and the initial conditions are

$$h(x,0) = \left(1 \cdot \cos\left(\frac{x}{8}\right)\right)\left(1 + \sin\left(\frac{x}{8}\right)\right), \tag{2.2}$$

and

$$h(x,0) = \left(0.1 \cdot \cos\left(\frac{x}{8}\right)\right)\left(0.1 + \sin\left(\frac{x}{8}\right)\right). \tag{2.3}$$

Figure 2.1 presents the solutions in the time range $[1, 600]$ for the different amplitudes applied in the initial conditions Eqs. (2.2) and (2.3). It seems that the results are vibrating depending on the parameter value in the initial condition. In Fig. 2.1(a) it can be seen that $h(x,t)$ is between ± 1.3 and in Fig. 2.1(b) that it is between ± 0.6 which begin to smooth out in both cases. This examination suggests that the initial condition amplitudes affect only the early phases of the surface evolution, while later the surface tends to approach a flat state regardless of the initial amplitudes

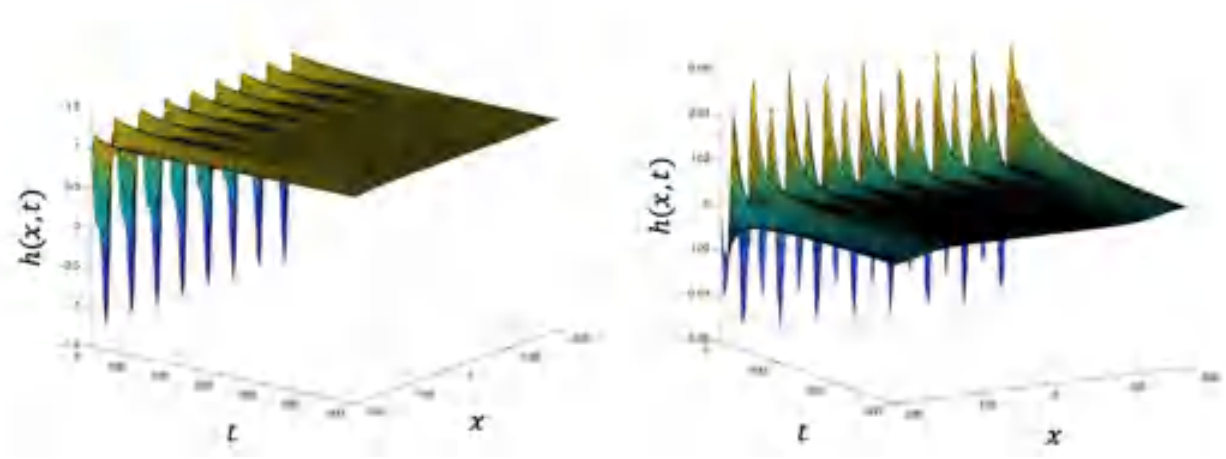

a b

Figure 2.1. The solutions of the KPZ equation (2.1) without noise term with initial conditions (2.2) and (2.3).

2.2. Results with Gaussian noise

Figure 2.4 presents the numerical results for the given parameters and $a = 1$ and for applying different initial condition amplitudes to Eq. (2.4) as follows

$$h(x,0) = \left(1 \cdot \cos\left(\frac{x}{8}\right)\right) \cdot \left(1 + \sin\left(\frac{x}{8}\right)\right). \quad (2.4)$$

and

$$h(x,0) = \left(0.1 \cdot \cos\left(\frac{x}{8}\right)\right) \cdot \left(0.1 + \sin\left(\frac{x}{8}\right)\right). \quad (2.5)$$

Figures 2.2 (a) and 2.2 (b) show almost the same structure. The only change is that if the amplitude is 1, the ripple appears, which can also be characterized by the maximum value of the amplitude.

ANALYSIS AND EVALUATION OF COATING CHARACTERISTICS

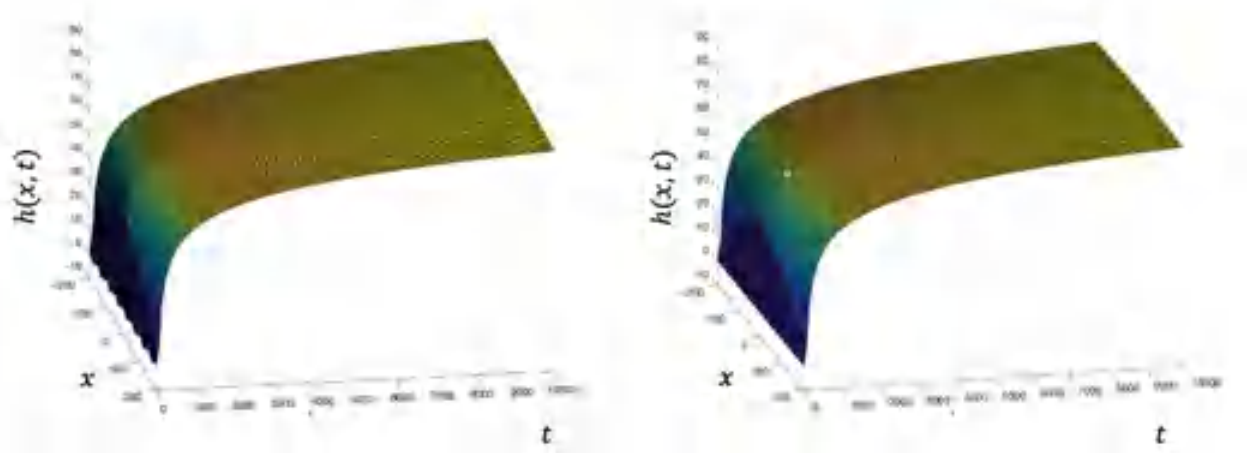

a b

Figure 2.2. The solutions of the KPZ Eq. (2.1) with Gaussian noise term with initial conditions (2.4) and (2.5).

Figure 2.3 shows the solutions of Eq. (2.1) with the same parameters. The figure shows the change in amplitude and the different representations of the graphs. We examine the effect of the strength of the Gaussian noise, providing $a = 0.1$ and $a = 0.01$ in the Gaussian noise term $\eta(x,t)$ together with the initial state

$$h(x,0) = \left(1 \cdot \cos\left(\frac{x}{8}\right)\right) \cdot \left(1 + \sin\left(\frac{x}{8}\right)\right). \quad (2.6)$$

It results the big wavy shape in the surface escaping while keeping increase amplitude of noise term.

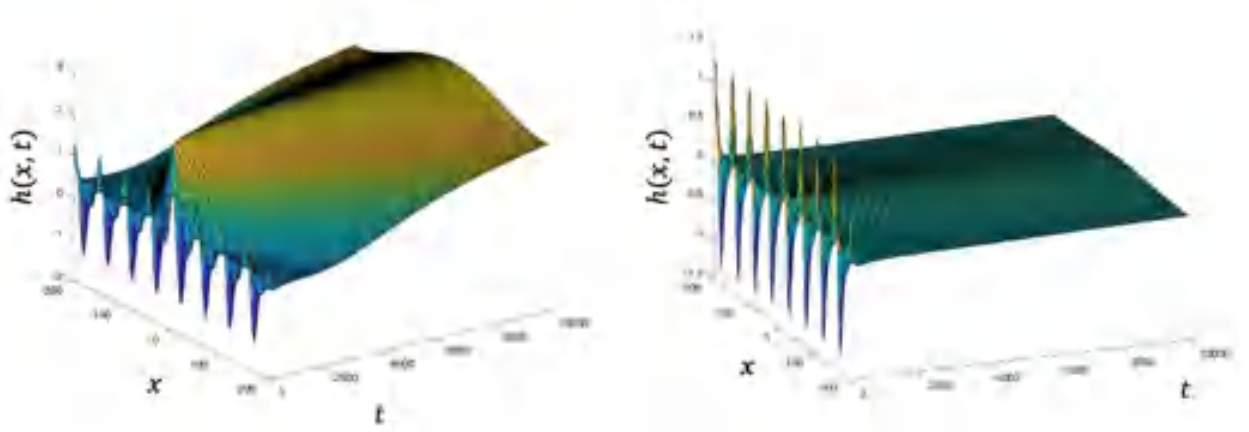

a b

Figure 2.3. The solutions of the KPZ Eq. (2.1) with Gaussian noise term with initial condition (2.6) and a=0.1 or a=0.01.

3. IMPACT OF NOISE TERMS

3.1. Results without noise term

Simulation data during the experiment are the following:

$$x \in [-100, 100],\ t \in [0, 1000],\ N = 100,\ \Delta t = 1/100, \tag{3.1}$$

where N denotes the number of division points on the x-axis and Δt is the time step.

In the resulted figures below the complete solutions of the original PDE (2.1) have been presented showing in different initial condition and various amplitudes. However, for simplicity, the parameters are chosen as $\nu = 0.1\ and\ 2,\ \lambda = 1$ and the initial condition is

$$h(x, 0) = \cos\left(\frac{x}{4}\right). \tag{3.2}$$

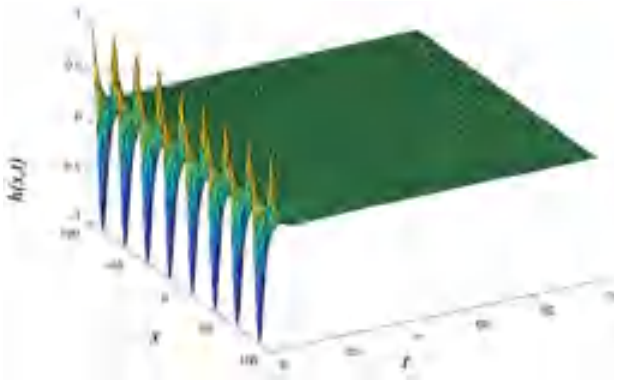

Figure 3.1. Solution to (3.1) KPZ equation without noise term for the parameter set $\nu = 0.1, \lambda = 1$.

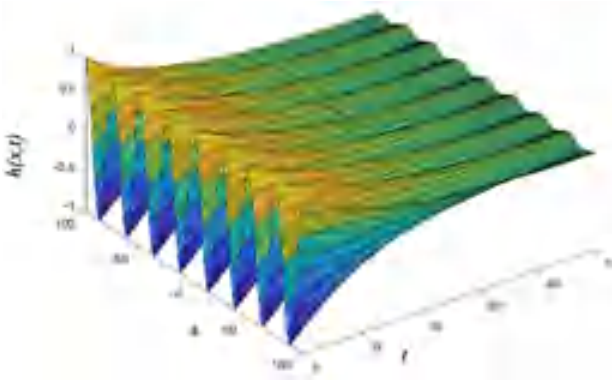

Figure 3.2. Solution to (3.2) KPZ equation without noise term for the parameter set $\nu = 2, \lambda = 1$.

Figure 3.1 and Figure 3.2 present the solutions in the time range $[1, 100]$ with initial condition (5.3). In the simulation result, on Fig. 3.1 the smoothing value is $\nu = 0.1$ and it can be seen that there is only initial condition effect at the beginning of the figure. This wavy surface continues till *t = 10*, then it becomes totally flat surface. Figure 3.2 represents the smoothing value which in our case equals to $\nu = 2$ and the surface waviness decreases slowly. However, this process creates a wavy surface for a long time, resulting in a significantly visible effect of the value ν.

3.2. Results with Gaussian noise

Figure 3.3 and Figure 3.4 present the solutions in the time range [1, 100] with initial condition (3.3). In the result of simulation Fig. 3.3, the smoothing value is $\nu = 0.1$ and it can be seen that

there is a small initial condition effect at the beginning of the figure then the Gaussian noise effect takes place. The Gaussian noise effect almost has not been affected by the initial condition. However, Figure 3.4 represents the smoothing value when it equals to $v = 2$ showing that surface waviness decreases slowly and effects to the Gaussian noise making it sharper curved. At the same time this process creates wavy surface for long time which gives significantly visible effect of value v.

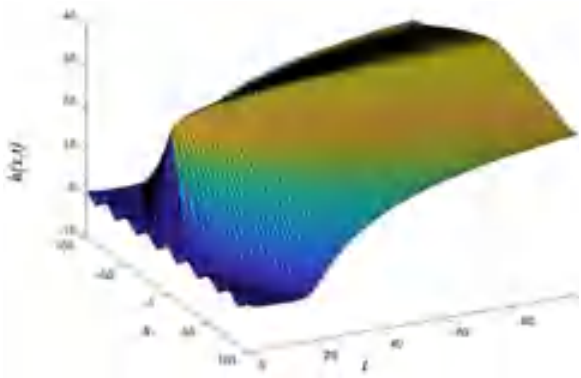

Figure 3.3. Solution to (3.3) KPZ equation without noise term for the parameter set $v = 2, \lambda = 1$.

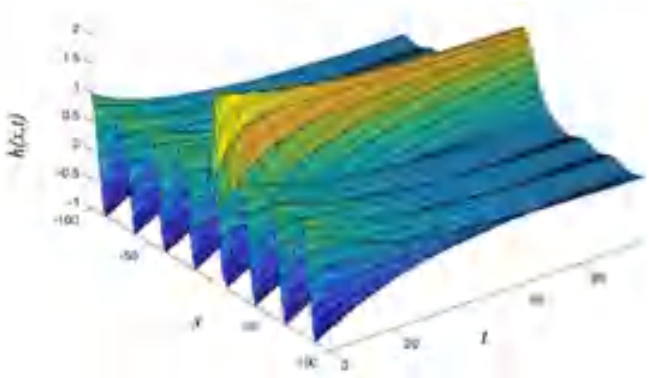

Figure 3.4. Solution to (3.3) The KPZ equation without a noise term was studied for the specified parameters v=2, λ=1.

3.3. Result with pink noise

Our first case is pink noise term $\eta(x,t) = \frac{a}{w}$.

The Figure 3.5 and 3.6 display the form of the shape function with varying physical parameters. At first, the solutions in both figures look the same. However, there is a significant increase on the Fig. 3.6 in a small time t. In other word the solution has an initial increase when the parameters v and λ are lower. As time goes the surface formation tend to reach flat surface with a small curve in the centre, which shows the pink noise effect along the surface.

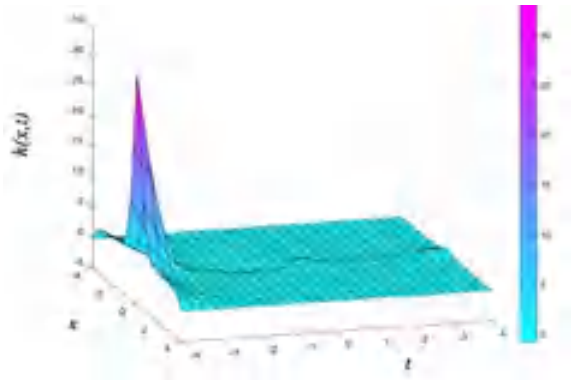

Figure 3.5 presents the solution of the KPZ equation that includes a pink noise term, for a specific set of parameters v=a=1 and λ=2. Here, initial condition is $h(x,0) = 0$.

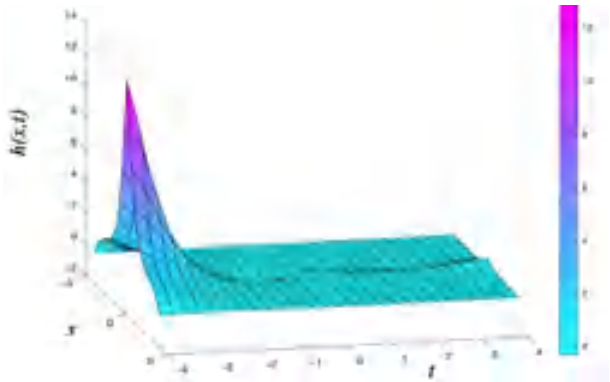

Figure 3.6. The solution of the KPZ equation with pink noise is depicted in Figure 5.5, with the specified parameters v=3,a=1 and λ=4. Here, initial condition is $h(x,0) = 0$.

3.4. Result with white noise

Our second case leads to the white noise term $\eta(x,t) = a\, w^0$. Figures 3.7 and 3.8 show the shape for the white noise. The different feature of this noise term from the pink noise is twice higher time of execution. However, when the parameters ν and λ are higher, the behaviour of the initial shape of the function is lower. While this effect reaches an arc shape after in small time t and it continuous on the surface till the end of the time.

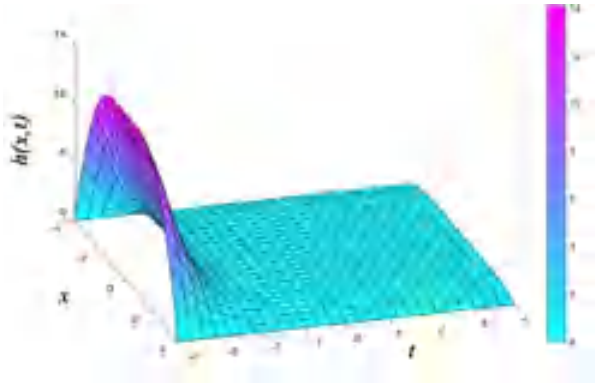

Figure 3.7. The KPZ equation solution with white noise, using the specified set of parameters v=a=1 and λ=2. Here, initial condition is $h(x,0) = 0$.

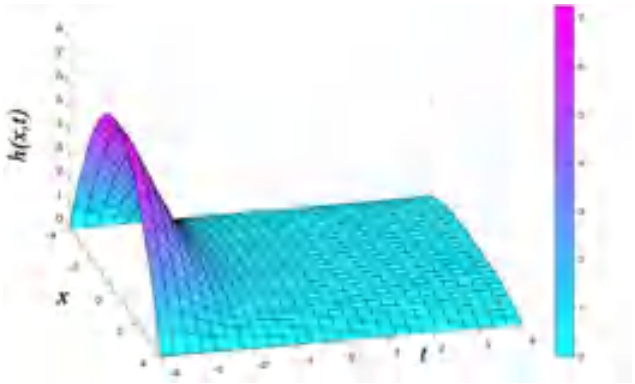

Figure 3.8. The KPZ equation solution with white noise, using the specified set of parameters v=3, a=1 and λ=4. Here, initial condition is $h(x,0) = 0$..

4. SOLUTION METHODS APPLYING DIFFERENTIAL FINITE ELEMENT METHODS

4.1. Forward Time Centered Space Scheme

In the paper [11], Moser et al. introduced spatial derivatives of the right-hand side of the KPZ Eq. (2.1). It was discretised using standard forward–backward differences on a cubic (4.1) grid with lattice constant Δx, which is also known as a forward time centred space (FTCS).

$$h_i^{n+1} = h_i^n + r(h_{i+1}^n + h_{i-1}^n - 2h_i^n) + \mu(h_{i+1}^n - h_{i-1}^n)^2 + \Delta t\, k(x,t) \qquad (4.1)$$

where Δt is the step size and $t_{i+1} = t_i + \Delta t$, $r = \frac{\upsilon \Delta t}{\Delta x^2}$ and $\mu = \frac{\lambda \Delta t}{8\Delta x^2}$ are the appropriate mesh ratios. We use only one array for the variable *h*, which has as many elements as the number of nodes. However, when we calculate h_i^{n+1}, the value of h_{i-1}^n is still necessary, thus we have to introduce an auxiliary temporary array variable to store the calculated values, and only after the completion of the loop can we load the new values h_i^{n+1} to the array. Therefore, with its speed, the seemingly simplest algorithm can still be surpassed, as we will show later.

4.2. Heun's method

The Heun method is an improved or a modified Euler's method applied in computational science and mathematics. It represents the explicit trapezoidal rule [30-31], which is a two-stage Runge–Kutta method. This method was originally proposed to solve ordinary differential equations (ODEs) with given initial conditions:

$$y'(t) = f(y(t), t), t(t_0) = y_0. \tag{4.2}$$

The procedure in this case is the following. At the first stage, Heun's method calculates the intermediate value y^{pred} and then the final approximation y^{n+1} at the next integration point:

$$\begin{aligned} y^{pred} &= y^n + hf(t^n, y^n), \\ y^{n+1} &= y^n + \frac{h}{2}[f(t^n, y^n) + f(t^{n+1}, y^{pred})]. \end{aligned} \tag{4.3}$$

Although the rate of convergence of Heun's method is two, thus it is usually more accurate than the simple explicit (Euler) method, its Courant–Friedrichs–Lewy (CFL) stability limit is unfortunately the same [32-33].

The predictor–corrector type that Heun's method applied to the KPZ equation reads as:

$$\begin{aligned} h_j^{pred} &= h_j^n + r\left(h_{j-1}^n + h_{j+1}^n - 2h_j^n\right) + \mu\left(h_{j+1}^n - h_{j-1}^n\right)^2 + k(x, t^n + \Delta t/2)\Delta t \\ h_i^{n+1} &= h_i^n + \frac{r}{2}\left(h_{i-1}^n + h_{i+1}^n - 2h_i^n + h_{j-1}^{pred} + h_{j+1}^{pred} - 2h_j^{pred}\right) \\ &\quad + \mu\left((h_{i+1}^n - h_{i-1}^n)^2 + \left(h_{j+1}^{pred} - h_{j-1}^{pred}\right)^2\right) + k\left(x, t^n + \frac{\Delta t}{2}\right)\Delta, \end{aligned} \tag{4.4}$$

where $\mu = \frac{\lambda \Delta t}{8\Delta x^2}$ and $k(x, t)$ is noise term. When Heun's method is implemented by two for loops, we need not only one extra array to store h_j^{pred}, but a temporary array as in the FTCs method. This makes a time step of Heun's algorithm slower and memory-consuming, although, to a much lesser extent than in the case of implicit methods.

4.3. Leapfrog–Hopscotch method

The leapfrog–hopscotch (LH) structure was first proposed and explained in our recent paper [27]. Similar to the original odd–even hopscotch (OEH) algorithm introduced five decades ago by Gordon [34] and Gourlay [35], one must divide the grid into two subgrids of odd and even nodes (light and dark blue dots in Fig. 4.1, respectively) such that the nearest neighbours of odd nodes are always even and vice versa. The calculation starts with a half-sized time step for the odd nodes using the initial h_i^0 values, symbolised by the green arrows in Fig. 4.1. Then, full time steps are made to calculate alternately the even and the odd nodes (light and dark blue arrows, respectively) until one reaches the final time, where the time step size must also be halved for odd nodes (orange arrows). One can see that in each step, the latest available *u* values of the neighbours (denoted by $h_{i\pm1}^{recent}$) are used, thus the method is explicit. We mention that this LH structure was thoroughly

examined for the diffusion equation [30]. According to a large number of numerical experiments, the UPFD formula is optimal for use in the zeroth time step and the symmetric $\theta = {}^{1}/_{2}$ formula in all other steps, thus we will apply only these formulas and we will call this concrete method (the LH time–space structure and the formulas) "the LH method". Due to the special symmetry of the time–space discretisation and the $\theta = {}^{1}/_{2}$, this method has excellent properties, as we will see in the following.

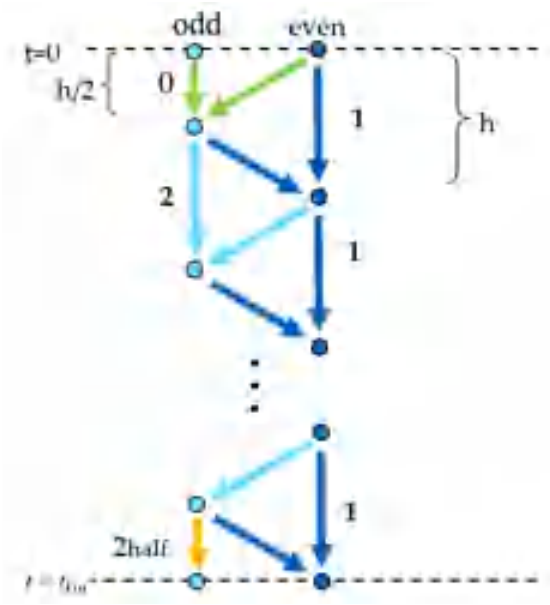

Figure 4.1. The new leapfrog–hopscotch structure.

We express the new value of the *h* variable in the following form in the case of the one space-dimensional KPZ equation [32-33] at the zeroth step:

$$h_i^{n+1} = \frac{2h_i^n + r(h_{i-1}^{recent} + h_{i+1}^{recent}) + \mu\,(h_{i-1}^{recent} - h_{i+1}^{recent})^2 + k(x, t^n + \Delta t/2)\Delta t}{2(1+r)} \qquad (4.5)$$

and at all other steps (denoted by 4.1 and 4.2 in Fig. 4.1.):

$$h_i^{n+1} = \frac{(1-r)h_i^n + r(h_{i-1}^{recent} + h_{i+1}^{recent}) + \mu\,(h_{i-1}^{recent} - h_{i+1}^{recent})^2 + k(x, t^n + \Delta t/2)\Delta t}{1+r} \qquad (4.6)$$

except the last, which is a half time step thus the substitution $\Delta t \to {}^{\Delta t}/_{2}, r \to {}^{r}/_{2}, \mu \to {}^{\mu}/_{2}$ must be performed in Eq. (4.6). We note that if $\mu = 0$ and $k = 0$ then one obtains back the original LH method's form developed for the diffusion equation. One can see that due to the time–space structure, the LH method does not use any extra arrays for the temporary values of *h*, and that is why it has less memory requirement, and it can be slightly faster than the simplest FTCS method.

ANALYSIS AND EVALUATION OF COATING CHARACTERISTICS

4.4. Comparison of different methods

For all three methods, with the parameters given in Eq. (4.7), the simulations were performed and the results are presented in Fig. 4.2.

$$\nu = 1,\ \lambda = 6,\ a = 1,\ c = 1 \tag{4.7}$$

Figure 4.2. Comparison of three different methods with various parameters in Eq. (4.7). The final time is $t_{fin} = 1$.

One can see in Fig. 4.2 that the curves are indistinguishable, which means that each method is accurate. The (global) numerical difference is the absolute difference of the numerical solutions h_i^{num} produced by the examined methods at final time t_{fin} for the KPZ equation: the FTCS scheme, the Heun method and the LH method for 10^{-5} and 10^{-4} time step size. For brevity, we denote this latter case, the LH method with 10^{-4} time step size as LH*.

In order to find an individual difference in the nodes or cells, we calculate the maximum and the average differences in the following ways:

$$D_i^{\text{FTCS,Heun}} = \left| h_i^{\text{FTCS}} - h_i^{\text{Heun}} \right|, \quad D_i^{\text{FTCS,LH}} = \left| h_i^{\text{FTCS}} - h_i^{\text{LH}} \right|, \quad D_i^{\text{Heun,LH}} = \left| h_i^{\text{Heun}} - h_i^{\text{LH}} \right|, \tag{4.8}$$

Average differences (L_1 errors)

$$L_1^{FTCS,Heun} = \sum_i \frac{D_i^{FTCS,Heun}}{Nx}, \quad L_1^{LH,LH*} = \sum_i \frac{D_i^{LH,LH*}}{Nx}, \text{ etc.} \tag{4.9}$$

Maximum differences (L_∞ errors)

$$L_\infty^{FTCS,Heun} = \max_i \{D_i^{FTCS,Heun}\},\ L_\infty^{LH,LH*} = \max_i \{D_i^{LH,LH*}\},\ \text{etc.} \tag{4.10}$$

In Tables 4.1 and 4.2, we show the average and the maximum differences of the methods, namely the FTCS, the Heun and the LH with two different time step sizes Δt. It is clear that due to enhanced stability, the LH method can be used with larger time step sizes for further investigation of the KPZ equation.

Table 4.1. Average difference without noise term.

t_{fin}	$L_1^{FTCS,Heun}$	$L_1^{FTCS,LH}$	$L_1^{Heun,LH}$	$L_1^{FTCS,LH*}$	$L_1^{Heun,LH*}$	$L_1^{LH,LH*}$
0.1	$3.48 \cdot 10^{-7}$	$3.47 \cdot 10^{-7}$	$2.70 \cdot 10^{-9}$	$3.86 \cdot 10^{-4}$	$3.88 \cdot 10^{-4}$	$3.88 \cdot 10^{-4}$
1	$5.45 \cdot 10^{-7}$	$5.42 \cdot 10^{-7}$	$2.45 \cdot 10^{-9}$	$4.30 \cdot 10^{-5}$	$4.34 \cdot 10^{-5}$	$4.34 \cdot 10^{-5}$
10	$3.20 \cdot 10^{-7}$	$3.19 \cdot 10^{-7}$	$1.10 \cdot 10^{-9}$	$3.20 \cdot 10^{-7}$	$8.38 \cdot 10^{-8}$	$8.38 \cdot 10^{-8}$

Table 4.2. Maximum difference without noise term.

t_{fin}	$\max_i\{D_i^{FTCS,Heun}\}$	$\max_i\{D_i^{FTCS,LH}\}$	$\max_i\{D_i^{Heun,LH}\}$	$\max_i\{D_i^{FTCS,LH*}\}$	$\max_i\{D_i^{Heun,LH*}\}$	$\max_i\{D_i^{LH,LH*}\}$
0.1	$6.91 \cdot 10^{-7}$	$6.93 \cdot 10^{-7}$	$8.56 \cdot 10^{-9}$	$6.66 \cdot 10^{-4}$	$6.66 \cdot 10^{-4}$	$6.66 \cdot 10^{-4}$
1	$1.32 \cdot 10^{-6}$	$1.31 \cdot 10^{-6}$	$6.57 \cdot 10^{-9}$	$1.47 \cdot 10^{-4}$	$1.48 \cdot 10^{-4}$	$1.48 \cdot 10^{-4}$
10	$3.24 \cdot 10^{-7}$	$3.23 \cdot 10^{-7}$	$1.12 \cdot 10^{-9}$	$4.66 \cdot 10^{-7}$	$1.52 \cdot 10^{-7}$	$1.51 \cdot 10^{-7}$

In addition, the total running time of the tested algorithms is presented in Table 4.3. It is shown that in various time t, the method's running time is different and the fastest is the leapfrog–hopscotch method for any time length. It is slightly faster than the FTCs method with the same time step size, as we mentioned before.

Table 4.3. Running time differences between the methods.

Methods	Running Time (s)		
	$t_{fin} = 0.1$	$t_{fin} = 1.0$	$t_{fin} = 10.0$
FTCS method, $\Delta t = 10^{-5}$	0.3232	2.9663	28.6288
Heun's method, $\Delta t = 10^{-5}$	0.6573	6.2133	73.8652
LH method, $\Delta t = 10^{-5}$	0.3135	2.5480	24.4324
LH method, $\Delta t = 10^{-4}$	0.0825	0.3105	2.4560

Note that when the time step size Δt is larger than 10^{-5}, the methods are unstable except for the LH method. This proves that our new method is not only the fastest, but also more stable even in larger time steps Δt. This numerical experiment demonstrated again that this new explicit method is very effective for the KPZ equation. We think that it will be very promising, especially in two or three space-dimensional numerical experiments since they include a large amount of the nodes or cells.

ANALYSIS AND EVALUATION OF COATING CHARACTERISTICS

4.5. Impact of different parameter values (without noise term)

In this section, we investigate the effect of different parameters, such as the coefficient ν, λ, a and t_{fin}. When one of the parameters are changed, all other parameters are fixed: $\nu = 1,\ \lambda = 6,\ a = 1$ and different final time t_{fin}. For the sake of verification, we still use not only the LH, but the FTCS and Heun's methods as well.

Figure 4.3 illustrates the solutions obtained with different methods for the linear diffusion parameter ν. It is clear that increasing the strength of the diffusion decreases the waviness of the surface. We note that when $\nu = 6.0$, the traditional methods (FTCS and Heun) are unstable, and they cannot be used even with this small-time step size.

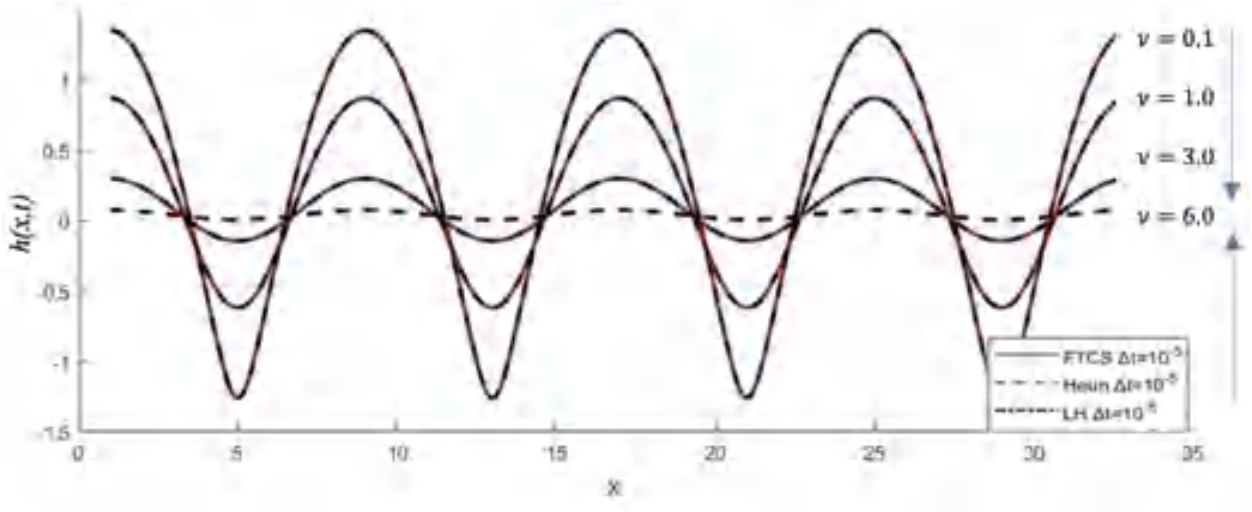

Figure 4.3. Numerical simulation of h for different diffusion coefficients υ with three methods.

In Fig.4.4, we illustrate the behaviour as a function of the nonlinear term parameter λ for final time $t_{fin} = 1$. One can see that the function is shifting to higher levels when the coefficient of the nonlinear term λ is increasing and the waviness of the function decreases.

ANALYSIS AND EVALUATION OF COATING CHARACTERISTICS

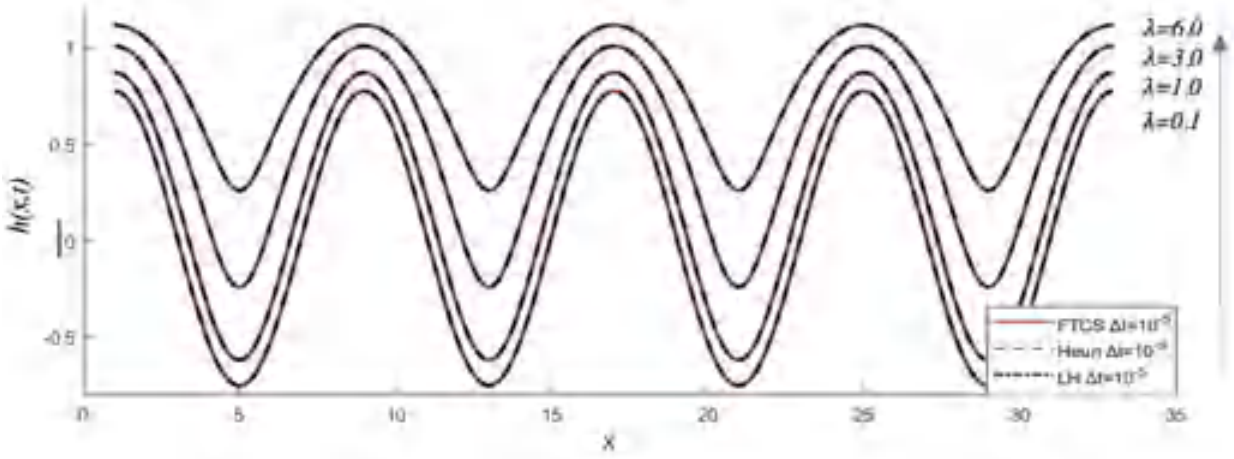

Figure 4.4. Numerical simulation of h for different nonlinear term coefficients λ with three methods.

Here, we are interested in the effect of the time on the used methods. In Fig. 4.5, we present the numerical solution of the discretised KPZ equation for different final times. Therefore, we perform the simulation for three different final times $t_{fin} = 0.1, 1.0$ and 10 with the parameters given in Eq. (4.10). One can conclude that the waviness of the surface is decreasing as time elapses.

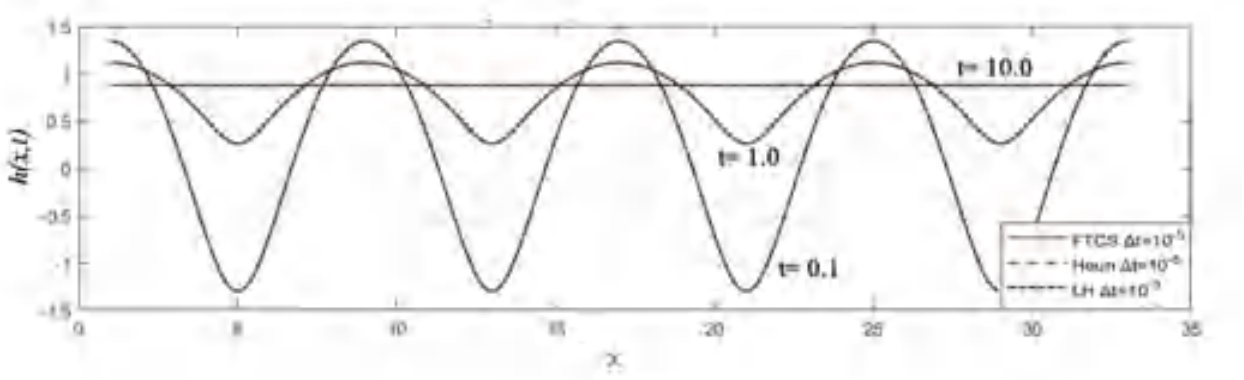

Figure 4.5. Numerical simulation of the system different time t with various methods

After examining each method with various parameters, we have more information on how the surface formation occurs. In the simulations, each increased parameter decreases the waviness of the function. However, as we mentioned above, if the linear term parameter has a higher value ($\upsilon \geq 6$), then only the LH method is stable, while the FTCS and Heun's methods are not stable.

5. SOLUTION METHODS APPLYING DIFFERENTIAL FINITE ELEMENT METHODS

5.1. Width function

The main attention of our work is the examination of the solutions to the KPZ equation in 1+1 dimension and the mean surface width or interface roughness of the height profile defined by

$$W(L,t) = \sqrt{\frac{1}{L}\int_0^L [h(x,t) - \langle h(L,t)\rangle]^2 dx}, \tag{5.1}$$

where $\langle h(L,t)\rangle = \int_0^L h(x,t)dx/L$ denotes the mean height at time t. For finite L, this quantity shows the scaling behaviour of many growth processes introduced by Family and Vicsek [36]

$$W(L,t) = L^{\alpha} W\left(\frac{t}{L^z}\right) \tag{5.2}$$

with the dynamical exponent z and the roughness exponent α. The scaling function has the limits $\mathrm{W}(y) \to 1$ for $y \to \infty$ and $\mathrm{W}(y) \sim y^{\beta}$ for $y \ll 1$ as $y = \frac{t}{L^z}$ The exponent β called growth exponent is given by $\beta = \alpha/z$. The saturation scales are as L^z, and the saturation width is proportional to L^{α} [10]. In 1+1 dimension, the KPZ equation holds $\alpha = 1/2$ and $z = 3/2$, thus, verifying the general Galilean invariance scaling relation $\alpha + z = 2$ [25]. The ratio of these values yields $\beta = 1/3$.

Initially, the authors [32] introduced spatial derivatives for the right-hand side of the KPZ equation (2.1). A discretized method was used that includes standard forward-backward differences for a cubic grid with a lattice constant Δx

$$h_i^{n+1} = h_i^n + \frac{\Delta t}{\Delta x^2}\left[\nu(h_{i+1}^n + h_{i-1}^n - 2h_i^n) + \frac{\lambda}{8}(h_{i+1}^n - h_{i-1}^n)^2\right] + \sqrt{\frac{2D}{\Delta x^d}}\sqrt{12\Delta t}\,\eta_i^n. \tag{5.3}$$

The most accurate result was obtained for Eq. (5.3) using Euler's method when $d = 1$ or $d = 2$. The results were similar and comparable to simulated results of another author [33]. However, for $d = 3$, the simulation showed the limitation of this method. Based on the previous simulation results, we apply for $d = 1$ in the present numerical experiments.

5.2. The numerical method applied for the KPZ equation in 1+1 dimension

The topic of discussion is the KPZ growth in (1+1) dimensions with temporal correlation, followed by an examination of the scaling results. We review existing numerical results and compare them with our simulation results. Furthermore, we perform several numerical simulations for different diffusion coefficients ν, as well as for the nonlinear coefficient λ and for systems of larger size L while fixing the other parameters. All numerical results are compared with the results of previous works [37-38]. For the simulations to analyze the effect of different coefficient, we

used a computer to analyze the effect of different coefficients, a MacBook Air 1,6 GHz Dual-Core Intel Core i5, 8 GB 2133 MHz LPDDR3 and the MATLAB R2019b software (The MathWorks, Inc., Portola Valley, CA, USA).

The simulation shows that the discretized version of the temporal correlated KPZ equation in (1+1) dimension displays numerical divergence in the effective λ regime [39], making it impossible to observe the system's evolution past a certain time limit due to singular growth. In order to prevent numerical instability, the nonlinear term is replaced by an exponentially decreasing function, as proposed by Dasgupta et al. [21]

$$f(x) \equiv \frac{1 - e^{-cx}}{c}, \tag{5.4}$$

where c is an adjustable parameter. Therefore, the temporal correlated KPZ equation in (1+1) dimension is modified and takes the following form

$$h_i^{n+1} = h_i^n + v\frac{\Delta t}{(\Delta x)^2}[h_{i+1}^n - 2h_i^n + h_{i-1}^n] + \Delta t\frac{\lambda}{2c}\left[1 - e^{-c\left[\frac{h_{i+1}^n - h_{i-1}^n}{2\Delta x}\right]^2}\right] + \eta_i^n,$$
$$\eta_i^n = \sqrt{\frac{2D}{\Delta x^d}}\sqrt{12\Delta t}\cdot R(t). \tag{5.5}$$

In Eq. (5.6), $R(t)$ is a random number from a uniform distribution in the interval $[-1.0, +1.0]$. In our further investigations, $c = 0.1$, $d = 1$ and the spatial and temporal steps are $\Delta x = 1$ and $\Delta t = 10^{-3}$, respectively. Our initial work started from flat interface at $t = 0$ with periodic boundary conditions that were used in our previous paper for different discretized methods.

We use random numbers in our simulations that vary between $a = -1.0$ and $b = 1.0$, and

$$R(t) = a + (b - a)\cdot rand(\Delta t, \Delta x), \tag{5.6}$$

where $rand(t1, x1)$ returns a t1 by x1 array of random numbers where $t1, \ldots, x1$ indicate the size of each dimension.

5.3. The impact of *a* and *b* on the surface growth

First, we investigate the morphology of the solutions to (5.5) when different lower and upper limits are applied in $R(t)$ in the noise term. The noise term values are random with different integers a and b.

$$\Delta x = 1,\ \Delta t = 10^{-3},\ \lambda = 1,\ \nu = 0.01,\ L = 1128,\ c = 0.1,\ D = 1,\ t = 100\ s. \tag{5.7}$$

ANALYSIS AND EVALUATION OF COATING CHARACTERISTICS

For different a and b, Fig. 5.1 shows the implementations for random numbers in the noise term for Eq. (5.5) with parameters fixed in (5.7). When the values of a are -0.5 or -1 and for b is 0.5 or 1, it can be seen that the height of the surface $h(x,t)$ formation is very high, reaching 4020. However, it is obvious from Fig. 5.1 that increasing the values of a and b also increases the surface roughness. For a =0 and b=0.5, we obtained the smallest roughness and for a =-1, b =1, the roughest surface structure. We note that the application of different parameters of a and b has an effect on the surface height and it can cause sudden increase of $h(x,t)$. Fortunately, the use of the equal a and b values show relatively similar surface formation height $h(x,t)$ as in other former research papers.

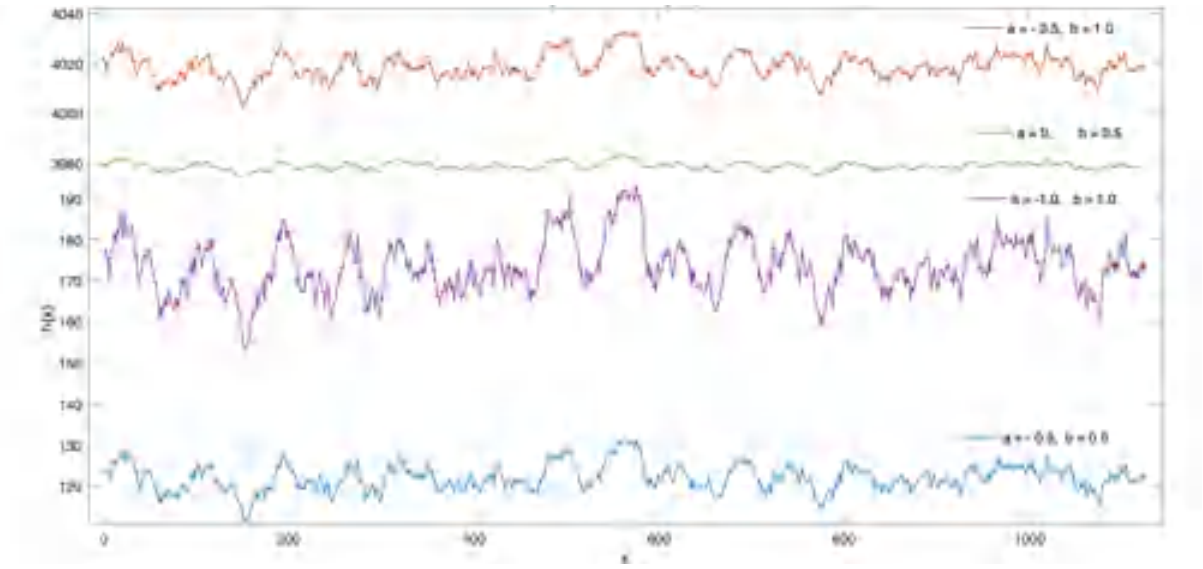

Figure 5.1. The plots of the solutions to the KPZ equation in (1+1) dimension at a growth time $t = 100$ *with parameters fixed in (5.7),* $\lambda = 1$*, and random numbers in the noise term that oscillate between* $a \in [-1.0, 0]$, $b \in [0.5, 1]$.

In the Fig. 5.2, the surface width $W(t)$ is plotted using the Eq. (5.7) and different pairs of a and b in the noise term. It shows that an increase of for $|a|$ and b, increases the surface width function as does the surface roughness.

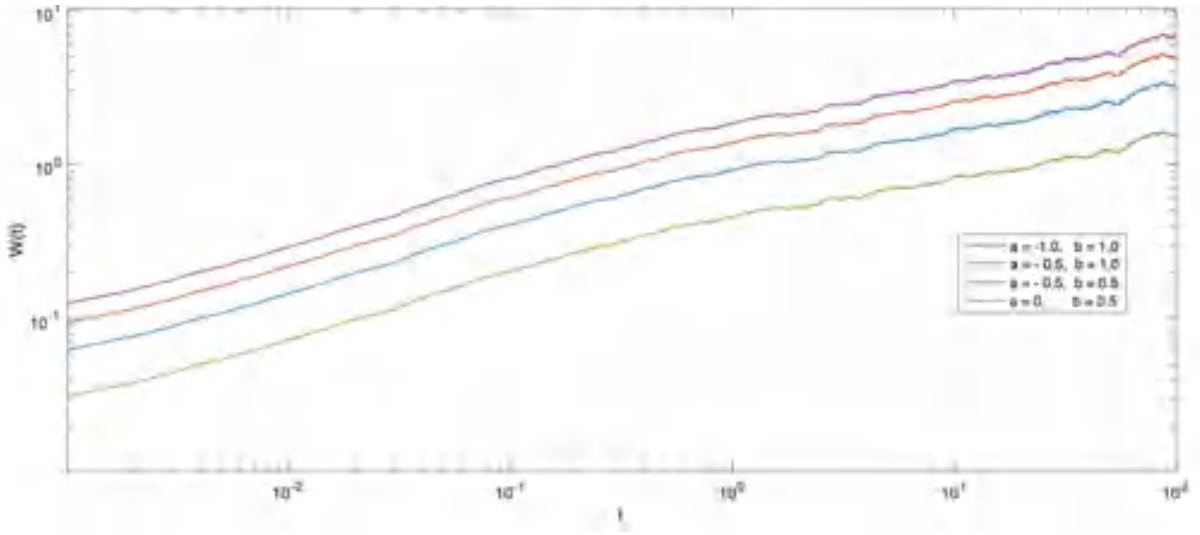

Figure 5.2. Log-log plot of the surface width $W(t)$ *for parameters fixed in (5.7),* $t = 100$ *and the random numbers in the noise term that oscillate between* $a \in [-1.0, 0]$, $b \in [0.5, 1]$.

5.4. The impact of ν and λ

The Kardar-Parisi-Zhang (KPZ) equation is a mathematical model that describes the behavior of randomly growing surfaces. The equation involves several parameters, including the roughness exponent (ν) and the growth exponent (λ).

Overall, the values of ν and λ in real experiments depend on the specific physical system being studied and the experimental conditions. The KPZ equation has been found to be a useful tool for describing the behavior of growing surfaces in a wide range of systems, and further studies are needed to better understand the relationship between the KPZ parameters and the behavior of different physical systems.

In this section, various smoothing ν and nonlinear λ parameters are investigated to show how they affect on the surface morphology. The simulation results are shown for the Eq. (5.5) with following fixed parameters

$$\Delta x = 1, \ \Delta t = 10^{-3}, \ L = 1128, \ c = 0.1, \ t = 100\ s. \qquad (5.8)$$

First, the interface profiles are plotted for the KPZ equation with different smoothening parameters ν. Figure 5.3 shows the various interface profiles for $\lambda = 1$ and $\nu = 0.01, 0.1, 0.5, 1, 2, 5, 10$. Figure 5.3 shows that the height of the interface profile decreases as the value of ν decreases. If the smoothening parameter ν is equal to 0.01, the height of surface roughness vibrating between $h(x,t) = 5500 \ldots 5700$ indicated in red in the figure. The least influenced height of the surface profile is shown in light blue ($\nu = 10$), which is below $h(x,t) = 5100$ and the smoothest compared to all other smaller parameters.

ANALYSIS AND EVALUATION OF COATING CHARACTERISTICS

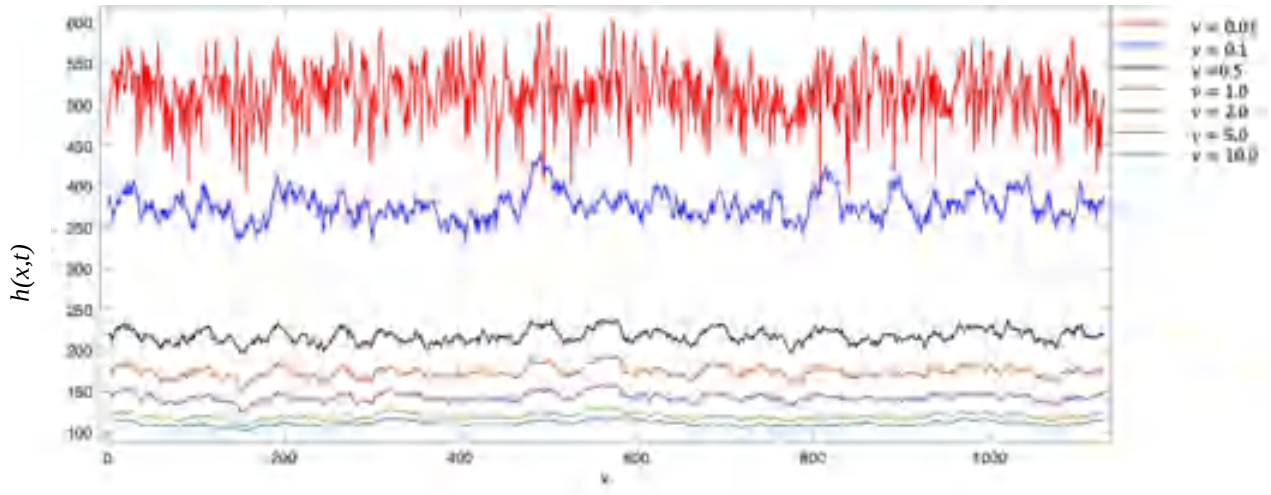

Figure 5.3. The shape of the KPZ equation in (1+1) dimension at the time of growth is studied $t = 100, \lambda = 1$ *and fixed parameters (5.8) for various parameters of* ν $(0.01, 0.1, 0.5, 1, 2, 5, 10)$.

The surface width function is presented on a log-log graph in Fig 5.4. Here, we fixed all the parameters as in (5.8) and keep changing the value of smoothening term ν from 0.01 to 10. Initially, each simulated result starts from the same point but during the time t they behave differently according to variety of the parameter ν. In the Fig. 5.4, the red line shows the highest width $W(t)$ in $\nu = 0.01$ that presents slightly curved line in the end. At the same time, it can be seen that increase of parameter ν decreases the width $W(t)$. However, the roughness of the lines is different that it is smoothy $\nu = 0.01$ and rough $\nu = 10$, respectively. Figure 4 also indicates that the slope of the function $W(t)$ agrees well with $t^{\frac{1}{3}}$ in the literature.

ANALYSIS AND EVALUATION OF COATING CHARACTERISTICS

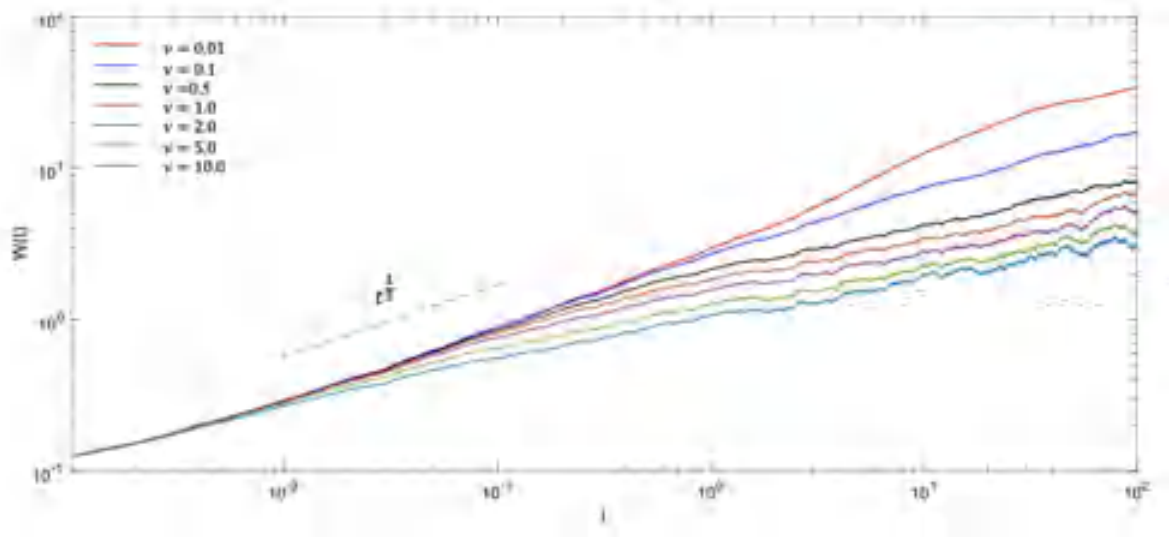

Figure 5.4. Log-log plot of the surface width $W(t)$ for fixed parameters (5.8), $\lambda = 1$ and $t = 100$. The parameter ν is between 0.01 and 10.0.

Figure 5.5 exhibits the plots of height $h(x)$ for various parameters λ of the nonlinear term ranging from 0.01 to 10. All the results obtained are obtained with a fixed smoothing parameter ν=0.01. Note that when ν is larger than 0.01, anomalous surface formation appears for different values of λ. However, the other fixed parameters were given in (5.8). When λ and ν are chosen to be equal, i.e., 0.01, the height of the interface profile h(x) is the lowest, as shown in Fig. 5.5 . The height of the interface profile $h(x)$ is uniformly oscillating. However, as the value of the nonlinear term λ increases, the surface roughness also increases and reaches the maximum value $h(x) = 1.2 \cdot 10^4$ for λ=10.

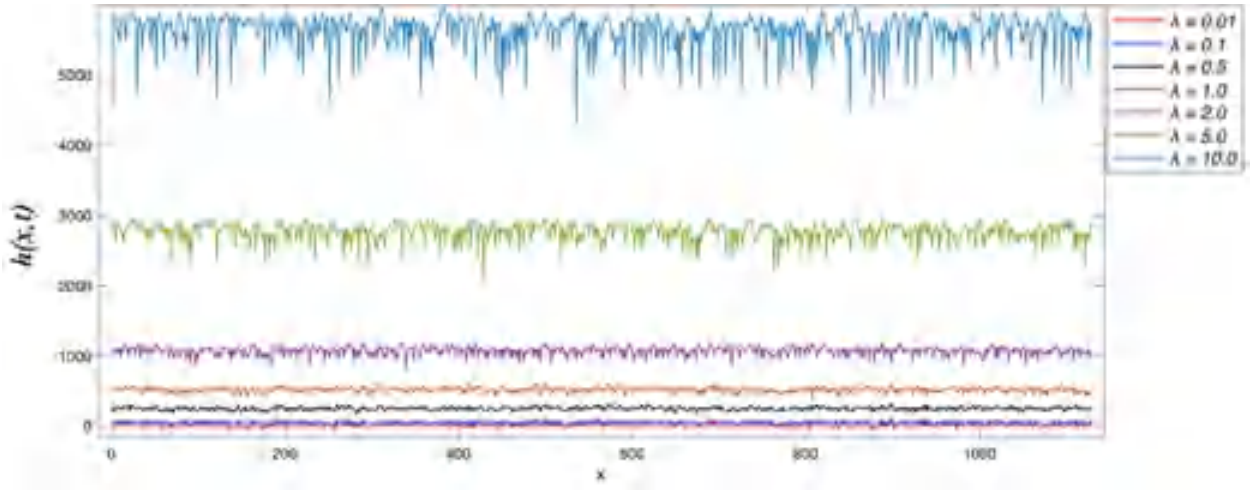

Figure 5.5. The shape of the KPZ equation in (1+1) dimension at the time of growth is studied $t = 100$, ν=0.01 and parameters in (7.8) for parameters of $\lambda = 0.01, 0.1, 0.5, 1, 2, 5, 10$.

ANALYSIS AND EVALUATION OF COATING CHARACTERISTICS

Fig. 5.6 presents log-log plot of the surface width $W(t)$ for fixed values of Eq. (5.8) and ν=0.01. It is similar to the Fig. 5.4 that initial point of all simulated results is started from the same points and increase till the certain time t. When the values of λ and ν are close/the same to each other, the interface width $W(t)$ is resemble too. However, increasing the value of nonlinear term λ, increase the interface width $W(t)$. It is obvious from the Fig. 5.6 that the highest curved and light blue (malibu) colored line represents the highest value of λ that equals to 10. Figure 5.6 also indicates that the slope of the function $W(t)$ agrees well with $t^{\frac{1}{3}}$ in the literature.

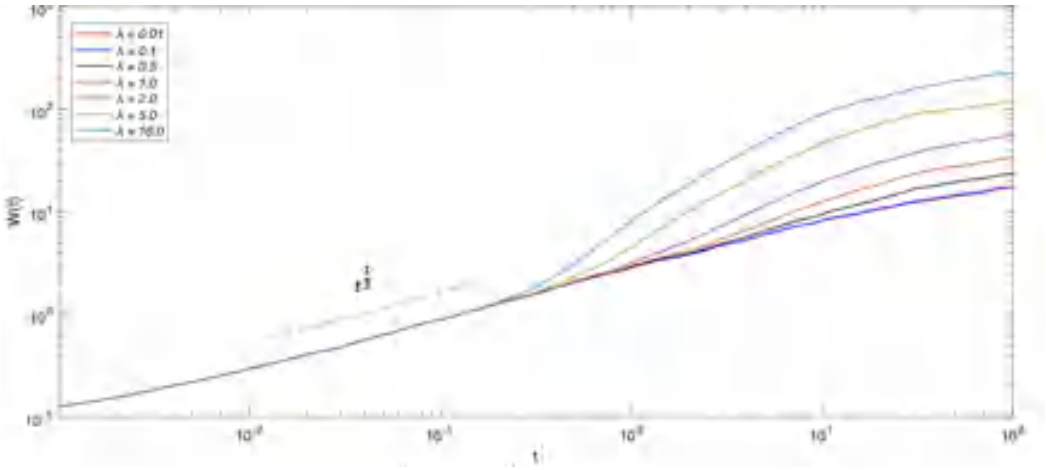

Figure 5.6. Log-log plot of the surface width $W(t)$ for parameters (5.8), time $t = 100$ and ν=0.01. The parameter of λ is between 0.01 and 10.0.

5.5. The impact of t on the slope of $W(t)$

To examine and compare the slope of the function $W(t)$, three different time periods $t = 10$, 100 and 500 are chosen. All the parameters in (5.8) are fixed except for the time and the value of the smoothing term ν. The Fig. 5.7 shows the slope results relation to the different values of the smoothing term ν, that is from 0.01, 0.05, 0.1, 0.5 … to 10. As it is presented in Fig. 5.7, the highest slope value that above 0.6 is obtained when the time was $t = 10$ for $\nu = 0.01$. It is shown by the blue line with circle. However, the values of slope significantly decreased till $\nu = 2$ then it continued decreasing smoothly. Consequently, the second highest slope is obtained when the time was $t = 100$ with the slope value between 0.55 and 0.6 and it is represented by the red starred line in the figure. Similarly, the above-mentioned behavior happened here too but it should be noted that slope values are higher for $t = 100$ than $t = 10$. Interestingly, the longest time that was $t = 500$ showed fluctuated result between 0.35 and 0.5 for along the ν values. It is illustrated by black line and "×"

Our examination of the slope of $W(t)$ shows that as t increases, the numerical results come closer and closer to the theoretical value of 1/3. For small t the slope is less than 1/3.

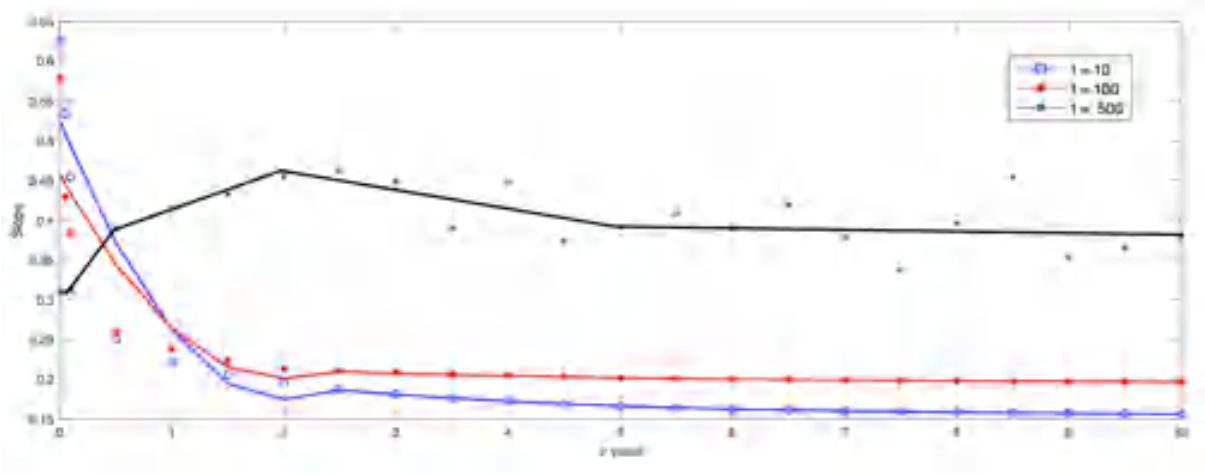

Figure 5.7. The width function's slope for the values of $\nu = (0.01, 0.05, 0.1, 0.5 \ \ldots \ 10)$ $t = 10, 100, 500$ *for the fixed* $\lambda = 1$. *All other parameters are given in (5.8).*

In Fig. 5.8, the slope of $W(t)$ is plotted for different nonlinear term values λ $(0.01, 0.05, 0.1, 0.5 \ \ldots \ 10)$ and time lengths $t = 10, 100$ and 500. It is shown that the highest slope belongs to the smallest time $t = 10$. It starts at 0.45 and increases significantly to 1.2 then levels off. Figure 5.8 shows that the near-constant slope decreases with increasing time t.

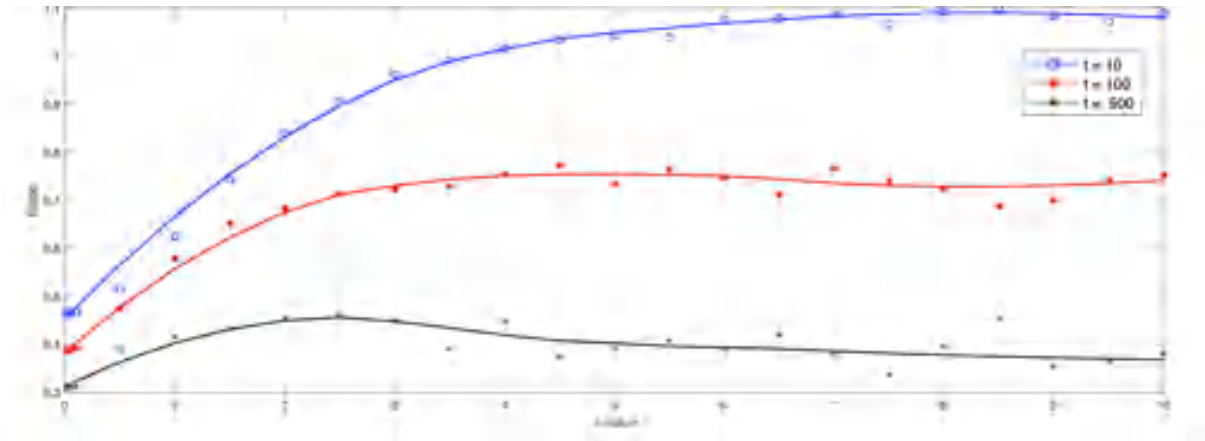

Figure 5.8. The width function's slope for different values of λ $(0.01, 0.05, 0.1, 0.5 \ \ldots \ 10)$ *in various time length* $t = 10, 100, 500$ *for the fixed* $\nu = 0.01$. *All other used parameters are given in the Eq. (5.8).*

5.6. The impact of *L*

Figure 5.9 shows the data obtained for different sizes of L lengths between 128 and 1024. These were obtained with a simulation run time of $t = 10^4, \lambda = 1, \nu = 1$. In all cases we started with a flat surface at t = 0. The data obtained for the (1+1)-dimensional KPZ equation confirm the Vicsek and Family scaling (5.2) for systems of different L sizes.

ANALYSIS AND EVALUATION OF COATING CHARACTERISTICS

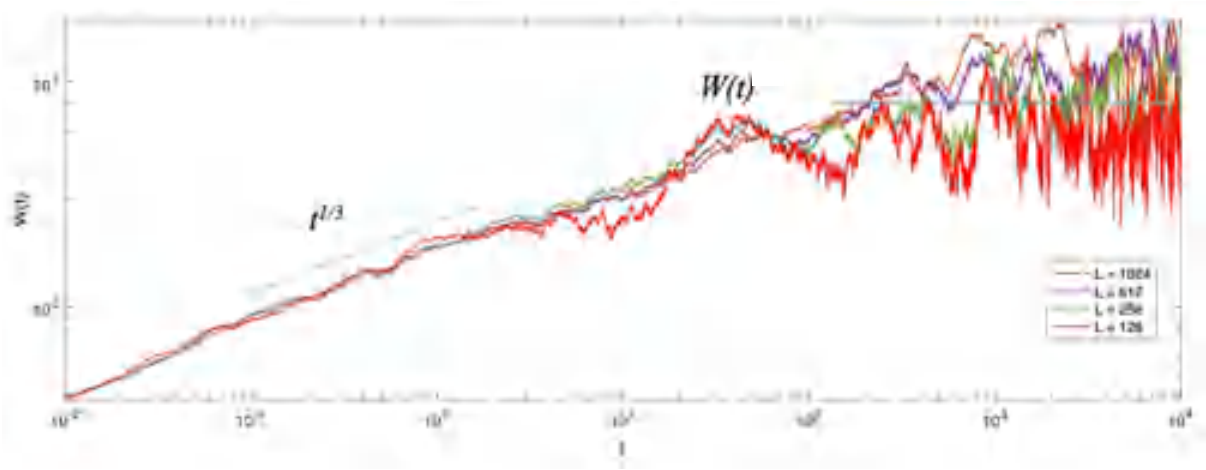

Figure 5.9. The log-log plot of width function in different linear system sizes L between 128 and 1024. Here, fixed parameters are: $\Delta x = 1, \Delta t = 10^{-2}, \lambda = 1, \nu = 1,\ c = 0.1, t = 10^4\ sec.$ *The dashed line shows a power-low with exponent 1/3.*

Figure 5.9 shows that the different linear system size L affects the slope of the width function. We started our numerical simulation with a system size of L = 1024, which is indicated in brown. The initial point of the line increases steadily, but after a certain time t oscillation started. When we reduce the system size L to 128, denoted by red, the oscillation starts early and the magnitude of the oscillation is at its maximum.

The impact of the random values in the noise term, the two parameters, a and b, on the surface growth of the 1+1 dimensional KPZ equation described by Eq. (5.6) in the presence of noise with different lower and upper limits in $R(t)$ is investigated. The results, shown in Figs. 5.1 and 5.2, demonstrate that increasing the values of a and b increases the surface roughness, and that the use of equal values of a and b results in relatively similar surface formation heights as compared to results of other researchers.

Moreover, the slope of the width function $W(t)$ is analyzed using simulations at different values of time ($t = 10$, 100, and 500), smoothing term (ν), and nonlinear term (λ). The results indicate that as t increases, the numerical results of the slope of $W(t)$ approximates well the theoretical value $1/3$ which confirms the Vicsek and Family scaling. Figures 5.7 and 5.8 show the relationship between different time lengths and smoothing/nonlinear term values and their effect on the slope of $W(t)$. The effect of different linear system sizes (L) on the slope of the width function is given. The simulation shows that as L decreases, the oscillation starts earlier and is more pronounced.

6. NEW SCIENTIFIC RESULTS – THESES

T1. I analyzed the numerical solutions to the one-dimensional KPZ equation using MATLAB with various initial condition amplitudes a and noise terms. The results showed that noise terms produced similar surface shapes regardless of the initial condition amplitude, and the presence of Gaussian noise is not observable at high initial conditions amplitude.

I investigated three power-law-type noises w^n with exponents of $-1, 0, 1$, called pink, white and blue noise respectively including Gaussian and Lorentzian noises. In order to observe and better understand certain physical phenomena, I used the data obtained from these experiments and validated a mathematical model. Decreasing initial condition amplitude and noise term strength for the KPZ equation resulted smoother surface structure [S1, S2, S3].

T2. I examined KPZ equation in one spatial dimension using the leapfrog–hopscotch (LH), standard forward time centered space (FTCS) scheme and the Heun methods. All methods are verified with analytical solution from at $t = 1$ as the initial condition and the Dirichlet boundary conditions. I showed that the average and the maximum differences of the methods, namely the FTCS, the Heun and the LH with two different time step sizes Δt. I found that FTCS and the Heun's methods are usually unstable above $\Delta t = 2 \times 10^{-5}$ (the concrete threshold for stability depends on the parameters such as ν, λ, a and Δt), while the LH method was stable in all numerical experiments. It can be unstable only if the nonlinear term λ are much higher than the linear coefficient ν and there are spike-like pillars or grooves. Therefore, even if the LH method is not unconditionally stable for the KPZ equation, it is obvious that it has much better stability properties than the conventional explicit methods [S4].

T3. I compared the impact of Gaussian and Brownian noises for the solutions of KPZ equation for various coefficients such as: ν, λ, a and t. I simulated two different noise terms with different parameters like linear, nonlinear and noise term amplitude. The effect of each applied parameter presented and discussed below:

ANALYSIS AND EVALUATION OF COATING CHARACTERISTICS

When the noise term amplitude is set to $a = 1$, the Brownian noise term has a greater effect than the Gaussian noise term.

- Increasing the simulation time t_{fin} from 1 to 10 showed that the effect of the Brownian noise term remains stronger than the Gaussian noise term, even at higher noise amplitudes.
- I also examined the impact of parameters ν and λ on the method. When the diffusion term's value is high at $\nu = 3.0$ and the nonlinear term has a low value at $\lambda = 0.1$ the surface shape closely resembles a sine wave.
- The Brownian noise term is affected by the increased linear term parameter ν, while the Gaussian noise term remains unchanged [S4].

T4. I discussed and numerically simulated the growth height of the KPZ equation using numerical method proposed by Dasgupta et al. [16]. I used random numbers $R(t)$ as a noise term that vary between $a = -1.0$ and $b = 1.0$. I found out that increasing the values of a and b increases the surface roughness. Consequently, the equal values of a and b results in relatively similar surface formation heights comparing to other researchers. In addition, I compared and investigated impacts of linear, nonlinear term parameters and different time to the height of the function. I got that increase of ν decreases oscillation level but increase the height of the function. In contrast, $\lambda = 0.01 \ldots 10.0$ and time $t = 1.0 \ldots 10.0$ increase the surface roughness [S6].

T5. I investigated impacts of ν linear, λ nonlinear parameters and time t to the surface width $W(t)$. I got that increase of ν that decrease surface width but oscillation level rised. The impact of t on the slope of the surface width $W(t)$ for ν and $\lambda = (0.01, 0.05, 0.1, 0.5 \ldots 10)$ simulated and calculated. The numerical results of the slope of surface width $W(t)$ approximates well to the theoretical value $1/3$ which confirms the Vicsek and Family scaling for systems of different sizes. We showed the relationship between different time lengths and smoothing/nonlinear term values and their effect on the surface slope of $W(t)$. The effect of different linear system sizes (L) on the slope of the surface width function is given. The simulation shows that as L decreases, the oscillation starts earlier and is more pronounced [S6].

7. LIST OF PUBLICATIONS RELATED TO THE TOPIC OF THE RESEARCH FIELD

[S1] O. Sayfidinov, G. Bognár, *Review on Relationship Between the Universality Class of the Kardar-Parisi-Zhang Equation and the Ballistic Deposition Model*, International Journal of Applied Mechanics and Engineering, vol. 26, no. 4, pp. 206–216, 2021, doi: 10.2478/ijame-2021-0060.

[S2] O. Sayfidinov, G. V. Bognár, *Numerical Solutions of the Kardar-Parisi-Zhang Interface Growing Equation with Different Noise Terms*, in Vehicle and Automotive Engineering 3, K. Jármai and K. Voith, Eds. Singapore: Springer Singapore, 2021, pp. 302–311. doi: 10.1007/978-981-15-9529-5_27.

[S3] O. Sayfidinov, G. Bognár, *One Dimensional Kardar-Parisi-Zhang Equation in Various Initial Condition Amplitudes*, J. Adv. App. Comput. Math., vol. 7, pp. 32–37, 2020, doi: 10.15377/2409-5761.2020.07.5.

[S4] O. Sayfidinov, G. Bognár, E. Kovács, *Solution of the 1D KPZ Equation by Explicit Methods*, Symmetry, vol. 14, no. 4, p. 699, 2022, doi: 10.3390/sym14040699.

[S4] O. Sayfidinov, G. Bognár, *Kardar-Parisi-Zhang interface growing equation with different noise terms*, presented at the International conference of numerical analysis and applied mathematics ICNAAM 2020, Rhodes, Greece, 2022, p. 290006. doi: 10.1063/5.0081584.

[S5] O. Sayfidinov, G. Bognár, *Dynamics of surface roughening in 1+1 dimensional Kardar-Parisi-Zhang growth with a random noise term*. Submitted to journal.

8. LITERATURE CITED IN THE THESES BOOKLET

[1] M. Kardar, G. Parisi, Y.-C. Zhang, *Dynamic Scaling of Growing Interfaces*, Phys. Rev. Lett., vol. 56, no. 9, pp. 889–892, 1986, doi: 10.1103/PhysRevLett.56.889.

[2] T. Halpin-Healy, Y.-C. Zhang, *Kinetic roughening phenomena, stochastic growth, directed polymers and all that. Aspects of multidisciplinary statistical mechanics*, Physics reports, vol. 254, no. 4–6, pp. 215–414, 1995, https://doi.org/10.1016/0370-1573(94)00087-J

[3] P. Meakin, *The growth of rough surfaces and interface*, Physics Reports, vol. 235, no. 4–5, pp. 189–289, 1993, doi: 10.1016/0370-1573(93)90047-H.

[4] G. Bognár, *Roughening in Nonlinear Surface Growth Model*, Applied Sciences, vol. 10, no. 4, pp 1-10 Paper 1422. 2020, doi: 10.3390/app10041422.

[5] I. F. Barna, G. Bognár, L. Mátyás, M. Guedda, K. Hriczó, *Analytic solutions of the two-dimensional Kardar-Parisi-Zhang growing equation*, AIP Conference Proceedings 2293, 280002, 2020.

[6] G Bognár, I. F. Barna, K Hriczó, *Investigation of roughening in nonlinear surface evaluation models*, AIP Conference Proceedings 2293, 280004, 2020.

[7] I. F. Barna, G. Bognár, L. Mátyás, M. Guedda, K. Hriczó, *Travelling-wave solutions of the Kardar-Parisi-Zhang interface growing equation with different kind of noise terms*, AIP Conference Proceedings 2293, 280005, 2020.

[8] I. F. Barna, G. Bognár, L. Mátyás, M. Guedda, and K. Hriczó, *Analytic Traveling-Wave Solutions of the Kardar-Parisi-Zhang Interface Growing Equation with Different Kind of Noise Terms*, Springer Proceedings in Mathematics and Statistics (2194-1009 2194-1017): vol. 333 pp 239-253, 2020.

[9] G. Bognár, M. Guedda, K. Hriczó, L. Taourirte, *Instabilities in certain one-dimensional singular interfacial equation*, Physica Scripta vol. 95 no. 3, 035001, 2020.

[10] J. G. Amar, F. Family, *Numerical solution of a continuum equation for interface growth in 2+ 1 dimensions*, Physical Review A, vol. 41, no. 6, p. 3399, 1990, https://doi.org/10.1103/PhysRevA.41.3399.

[11] K. Moser, J. Kertész, D. E. Wolf, *Numerical solution of the Kardar-Parisi-Zhang equation in one, two and three dimensions*, Physica A: Statistical Mechanics and its Applications, vol. 178, no. 2, pp. 215–226, 1991, https://doi.org/10.1016/0378-4371(91)90017-7.

[12] K. Moser, D. E. Wolf, *Vectorized and parallel simulations of the Kardar-Parisi-Zhang equation in 3+ 1 dimensions*, Journal of Physics A: Mathematical and General, vol. 27, no. 12, p. 4049, 1994, doi: 10.1088/0305-4470/27/12/013.

[13] M. S. Li, *Surface growth with spatially correlated noise*, Phys. Rev. E, vol. 55, no. 1, pp. 1178–1180, Jan. 1997, doi: 10.1103/PhysRevE.55.1178.

[14] H. Jeong, B. Kahng, D. Kim, *Anisotropic Surface Growth Model in Disordered Media*, Phys. Rev. Lett., vol. 77, no. 25, pp. 5094–5097, 1996, doi: 10.1103/PhysRevLett.77.5094.

[15] Y. Tu, G. Grinstein, M. A. Muñoz, *Systems with Multiplicative Noise: Critical Behavior from KPZ Equation and Numerics*, Phys. Rev. Lett., vol. 78, no. 2, pp. 274–277, 1997, doi: 10.1103/PhysRevLett.78.274.

[16] C. Jayaprakash, F. Hayot, R. Pandit, *Universal properties of the two-dimensional Kuramoto-Sivashinsky equation*, Phys. Rev. Lett., vol. 71, no. 1, pp. 12–15, 1993, doi: 10.1103/PhysRevLett.71.12.

[17] J. Li, L. M. Sander, *Scaling properties of the Kuramoto-Sivashinsky equation*, Fractals, vol. 03, no. 03, pp. 507–514, 1995, doi: 10.1142/S0218348X95000436.

[18] M. Rost, J. Krug, *Coarsening of surface structures in unstable epitaxial growth*, Phys. Rev. E, vol. 55, no. 4, pp. 3952–3957, 1997, doi: 10.1103/PhysRevE.55.3952.

[19] T. J. Newman, A. J. Bray, *Strong-coupling behaviour in discrete Kardar - Parisi - Zhang equations*, J. Phys. A: Math. Gen., vol. 29, no. 24, pp. 7917–7928, 1996, doi: 10.1088/0305-4470/29/24/016.

[20] C. Dasgupta, S. D. Sarma, J. M. Kim, *Controlled instability and multiscaling in models of epitaxial growth*, Physical Review E, vol. 54, no. 5, p. R4552, 1996, doi: https://doi.org/10.1103/PhysRevE.54.R4552.

[21] C. Dasgupta, J. M. Kim, M. Dutta, S. Das Sarma, *Instability, intermittency, and multiscaling in discrete growth models of kinetic roughening*, Phys. Rev. E, vol. 55, no. 3, pp. 2235–2254, 1997, doi: 10.1103/PhysRevE.55.2235.

[22] C.-H. Lam, F. G. Shin, *Anomaly in numerical integrations of the Kardar-Parisi-Zhang equation*, Phys. Rev. E, vol. 57, no. 6, pp. 6506–6511, Jun. 1998, doi: 10.1103/PhysRevE.57.6506.

[23] J. G. Amar, F. Family, *Deterministic and stochastic surface growth with generalized nonlinearity*, Phys. Rev. E, vol. 47, no. 3, pp. 1595–1603, 1993, doi: 10.1103/PhysRevE.47.1595.

[24] H. S. Wio, J. A. Revelli, R. R. Deza, C. Escudero, M. S. de La Lama, *Discretization-related issues in the KPZ equation: Consistency, Galilean-invariance violation, and fluctuation--dissipation relation*, Phys. Rev. E, vol. 81, no. 6, p. 066706, 2010, doi: 10.1103/PhysRevE.81.066706.

[25] H. S. Wio, M. A. Rodríguez, R. Gallego, J. A. Revelli, A. Alés, R. R. Deza, *d-Dimensional KPZ Equation as a Stochastic Gradient Flow in an Evolving Landscape: Interpretation and Time Evolution of Its Generating Functional*, Front. Phys., vol. 4, 2017, doi: 10.3389/fphy.2016.00052.

[26] H. S. Wio, M. A. Rodríguez, R. Gallego, *Variational approach to KPZ: Fluctuation theorems and large deviation function for entropy production*, Chaos, vol. 30, no. 7, p. 073107, 2020, doi: 10.1063/5.0006121.

[27] O. Niggemann, U. Seifert, *The Two Scaling Regimes of the Thermodynamic Uncertainty Relation for the KPZ-Equation*, J Stat Phys, vol. 186, no. 1, p. 3, 2022, doi: 10.1007/s10955-021-02845-8.

[28] C. Cartes, E. Tirapegui, R. Pandit, M. Brachet, *The Galerkin-truncated Burgers equation: crossover from inviscid-thermalized to Kardar–Parisi–Zhang scaling*, Phil. Trans. R. Soc. A., vol. 380, no. 2219, p. 20210090, 2022, doi: 10.1098/rsta.2021.0090.

[29] G. Hu, G. Orkoulas, P. D. Christofides, *Modeling and control of film porosity in thin film deposition*, Chemical Engineering Science, vol. 64, no. 16, pp. 3668–3682, 2009, doi: 10.1016/j.ces.2009.05.008.

[30] Á. Nagy, I. Omle, H. Kareem, E. Kovács, I. F. Barna, G. Bognár, *Stable, Explicit, Leapfrog-Hopscotch Algorithms for the Diffusion Equation*, Computation, vol. 9, no. 8, p. 92, 2021, doi: 10.3390/computation9080092.

[31] U. M. Ascher, L. R. Petzold, *Computer Methods for Ordinary Differential Equations and Differential-Algebraic Equations*, Library of Congress Cataloging-in-Publication Data, Philadelphia, 1998.

[32] E. Kovács, Á. Nagy, M. Saleh, *A Set of New Stable, Explicit, Second Order Schemes for the Non-Stationary Heat Conduction Equation*, Mathematics, vol. 9, no. 18, p. 2284, 2021, doi: 10.3390/math9182284.

[33] J. Muñoz-Matute, V. M. Calo, D. Pardo, E. Alberdi, K. G. van der Zee, *Explicit-in-time goal-oriented adaptivity*, Computer Methods in Applied Mechanics and Engineering, vol. 347, pp. 176–200, 2019, doi: 10.1016/j.cma.2018.12.028.

[34] P. Gordon, *Nonsymmetric Difference Equations*, Journal of the Society for Industrial and Applied Mathematics, vol. 13, no. 3, pp. 667–673, Sep. 1965, doi: 10.1137/0113044.

[35] A. R. Gourlay, *Hopscotch: a Fast Second-order Partial Differential Equation Solver*, IMA J Appl Math, vol. 6, no. 4, pp. 375–390, 1970, doi: 10.1093/imamat/6.4.375.

[36] F. Family, T. Vicsek, *Scaling of the active zone in the Eden process on percolation networks and the ballistic deposition model*, J. Phys. A: Math. Gen., vol. 18, no. 2, pp. L75–L81, 1985, doi: 10.1088/0305-4470/18/2/005.

[37] Z. Rácz, M. Siegert, D. Liu, M. Plischke, *Scaling properties of driven interfaces: Symmetries, conservation laws, and the role of constraints*, Phys. Rev. A, vol. 43, no. 10, pp. 5275–5283, 1991, doi: 10.1103/PhysRevA.43.5275.

[38] G. Costanza, *Langevin equations and surface growth*, Phys. Rev. E, vol. 55, no. 6, pp. 6501–6506, 1997, doi: 10.1103/PhysRevE.55.6501.

[39] D. Sergi, A. Camarano, J. M. Molina, A. Ortona, J. Narciso, *Surface growth for molten silicon infiltration into carbon millimeter-sized channels: Lattice–Boltzmann simulations, experiments and models*, Int. J. Mod. Phys. C, vol. 27, no. 06, p. 1650062, 2016, doi: 10.1142/S0129183116500625.

[40] G. Ódor, B. Liedke KH. Heinig, *Directed d-mer diffusion describing the Kardar-Parisi-Zhang-type surface growth*. Physical Review E. 2010 Mar 12;81(3):031112. https://doi.org/10.1103/PhysRevE.81.031112